II International Conference on Particle-based Methods - Fundamentals and Applications
PARTICLES 2011
E. Oñate and D.R.J. Owen (Eds)

CREEP BEHAVIOUR OF CONFINED LAYERS OF POLYHEDRAL GRAINS

J.C. Quezada*, F. Radjai† G. Saussine*

*Innovation and Research Department of SNCF
45 rue de Londres, 75379 Paris Cedex 8
e-mail: juan-carlos.quezada-guajardo@sncf.fr

†LMGC, Université Montpellier II
CC048 Place Eugène Bataillon, 34095 Montpellier
e-mail: franck.radjai@univ-montp2.fr

Key words: Creep, Contacts Dynamics, Thin Granular Layer, Statistical Variability

Abstract. By means of contact dynamics simulations, we investigate the creep deformation of a thin granular layer composed of irregular polyhedral particles under the action of a constant vertical overload applied on a horizontal wall on top of the layer. We show that the total deformation induced by the overload increases with the ratio between the vertical and confining horizontal stresses and the aspect ratio of the sample. The effect of the aspect ratio is a consequence of the mobilized wall-grain friction forces at the top and bottom boundaries, that lead to enhanced strength by stabilizing strong force chains at the center of the sample. We also evidence the influence of loading history due to strain-induced fabric change or inertial effects resulting from the instant application of the overload. The topology of the contact network evolves in close correlation with creep. In particular, the face/face contacts between polyhedral particles concentrate largest force chains and their number is an increasing function of creep. A crucial feature of a confined granular system is the statistical variability of the mechanical response that we analyzed for creep deformations by performing a large number of simulations for independent initial configurations. Our data indicate that the distribution of fluctuations with respect to the mean creep falls off exponentially.

1 Introduction

Granular media behaviour has been at the focus of several experimental studies. Examples are hopper flow, jamming-unjamming transition and granular avalanches [3, 11]. One of these phenomena is the creep in granular media under static overload. This creep involves axial deformation induced by the applied overload, allowing the system to explore

metastable configurations. This axial deformation produces in the granular material accumulated plastic deformations, know as settlement. Moreover, the mechanisms of creep in granular media are badly understood.

In many configurations, we can find a few numbers of grains in a composed layer, such as hopper flow, avalanches and railway ballast track, for example. These confined granular systems are the thin granular interfaces since its thickness is below the correlation length of contacts forces and particle displacement during a quasi-static flow [9].

In this paper, we present a numerical study of the mechanical behaviour of a confined layer under the action of a constant overload. We use the contacts dynamics method [5, 7, 2, 4, 10]. We focus on the settlement levels due to the creep deformation, under several applied overload and different initial configurations. We show the influence of the stress ratio, aspect ratio and loading history in the settlement. These results show intrinsic fluctuations, which is associated with the statistical variability of the mechanical response. Our data suggest that the distribution of mean creep fluctuations follow a decreasing exponential law.

2 Numerical Procedures

In this section, we briefly introduce the contact dynamics (CD) method with polyhedral particles as well as the numerical procedures used for the preparation of the numerical samples.

2.1 Contact dynamics method

The simulations were carried out by means of the contact dynamics (CD) method with irregular polyhedral particles [5, 7, 2, 4, 10]. The CD method is a discrete element approach for the simulation of nonsmooth granular dynamics with contact laws expressing basically the mutual exclusions and dry friction between particles without elastic or viscous regularization often used in explicit methods such as molecular dynamics or distinct element method introduced by Cundall and Strack [1]. Hence, this method is particularly adapted for the simulation of perfectly rigid particles. The nonsmoothness refers to various degrees of discontinuity in velocities arising in a system composed of rigid particles. In this method, the equations of motion for each particle are formulated as differential inclusions in which velocity jumps replace accelerations [6]. The unilateral contact interactions and Coulomb friction law are treated as complementarity relations or set-valued contact laws. The time-stepping scheme is implicit but requires explicit determination of the contact network. Due to implicit time integration, this scheme is unconditionally stable[1].

At a given step of time evolution, all kinematic constraints implied by frictional contacts

[1]For our simulations, we used the LMGC90 which is a multipurpose software developed in Montpellier, capable of modeling a collection of deformable or non deformable particles of various shapes by different algorithms [2, **?**], see www.lmgc.univ-montp2.fr/ dubois/LMGC90.

between particles are simultaneously taken into account, together with the equations of dynamics, in order to determine all velocities and contact forces in the system. This problem is solved by an iterative process pertaining to the non-linear Gauss-Seidel method, which consists of solving a single contact problem with other contact forces being treated as known, and iteratively updating the forces and velocities until a convergence criterion is fulfilled.

The determination of the contact set for irregular polyhedral particles proceeds in three steps. First, a "bounding box" method is used to sort a list of neighboring particle pairs. Then, for each pair, the overlaps are calculated through a 3D extension of the "shadow overlap method" [2, 12]. Several algorithms exist for overlap determination between convex polyhedra [8, 13]. In the case of an overlap, the contact plane is determined by means of the intersection between the two particles. This detection procedure is fairly rapid and allows us to simulate large samples composed of polyhedral particles.

The contacts between polyhedral particles belong to different categories, namely face-face, edge-face, vertex-face, edge-edge, vertex-vertex, vertex-edge. The vertex-vertex and vertex-edge contacts are rare. Face-face contacts are represented by three points, corresponding to three geometrical constraints, and thus will be referred below as *triple* contacts. The edge-face contacts are represented by two points and will be called *double* contacts. All other contacts are *simple* contacts represented by a single point. In the iterative procedure of determination of the contact forces and velocities, the points representing the contacts between two particles are treated as independent points but the resultant of the calculated forces are attributed to the contact with its application point located on the contact plane.

2.2 Sample preparation

We generate 32 numerical samples composed of 2700 perfectly rigid polyhedral grains. The grain shapes are taken from a library of 1000 digitalized ballast grains[2]. Each grain has at most 70 faces and 37 vertices and at least 12 faces and 8 vertices. Fig. 2 shows several examples of the polyhedral grains used in the simulations. The size of a grain is defined as two times the largest distance between the barycenter and the vertices of the particle, to which we will refer as the "diameter" of the particle. The grain sizes vary between 25 mm and 50 mm with 50% of diameter 25 mm, 34% of diameter 37.5 mm and 16% of diameter 50 mm. The bulk density of the grains is 2700 kg m^{-3}. The coefficient of friction between the grains is 0.8 for all samples. The normal and tangential coefficients of restitution are $\simeq 0$.

The preparation protocol consists in first pouring the grains into a cylindrical box with zero grain-wall friction. A rigid block of weight $W = 16$ kg is placed on top of the sample. Then, the cylinder is removed and a radial confining pressure of 80 kPa is applied on the sample by a uniform distribution of radial forces over the outmost grains

[2]The library was provided by the French Railway Company SNCF.

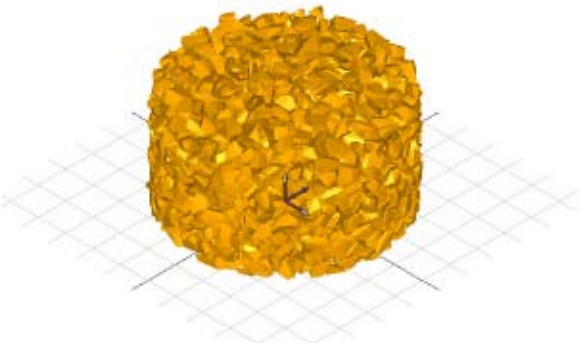

Figure 1: Snapshot of a numerical sample.

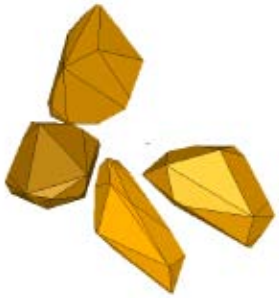

Figure 2: Four examples of polyhedral grains used in the simulations.

located on the periphery of the cylinder while keeping the bottom plane fixed. The sample obtained by this procedure is subjected to vibrations of small amplitude by applying a vertical sinusoidal displacement on the top wall. The vibrations last for about 0.4 s with a frequency of 10 Hz. Then, the vibration is stopped and the sample is allowed to relax to static equilibrium. The resulting sample has a height of $H_0 = 0.4$ m and a radius of $R \simeq 35$ cm. The applied protocol is fairly reproducible and the packing fraction ρ for the 32 samples is in the range $[0.610, 0.626]$. Fig. 1 shows a snapshot of a numerical sample.

The creep deformation is studied by applying a constant overload F on the top wall. In a series of simulations, 500 different values of F varying from 0.9 kN to 120 kN were. The deformation lasts until a stable equilibrium state is reached. The time step was $4.10^{-4}s$ in all simulations and at most 150 time steps were needed for full stabilization. The CPU time was $2.10^{-3}s$ per particle and per time step on a Dell computer of speed 3.16 GHz. The creep was also investigated by stepwise application of small overloads and with different values of a "pre-consolidation" overload; see below.

3 Creep deformation

Figure 3 shows the creep deformation δH of a sample subjected to different values of the overload F as a function of time. The total creep increases with η.

The total creep deformation ΔH depends on how the overload is applied. The same total overload may be applied in two or more steps. Let n be the number of steps. We find that $n\Delta H(F/n) < (n-1)\Delta H(F/(n-1)$. This implies that a quasi-staic compression of the sample should yield the lowest level of deformation. In other words, quasi-static loading provides the lower bound for creep deformation.

Fig. 4 displays the creep deformation $\Delta H(t)$ for different stepwise applications of a total overload of $F = 60$ kN.

The abrupt application of an overload leads to the inertial motion of the grains. The extra inertial forces, in addition to the total force $F + \textit{top wall weight} + \textit{sample weight}$ can be measured on the bottom wall.

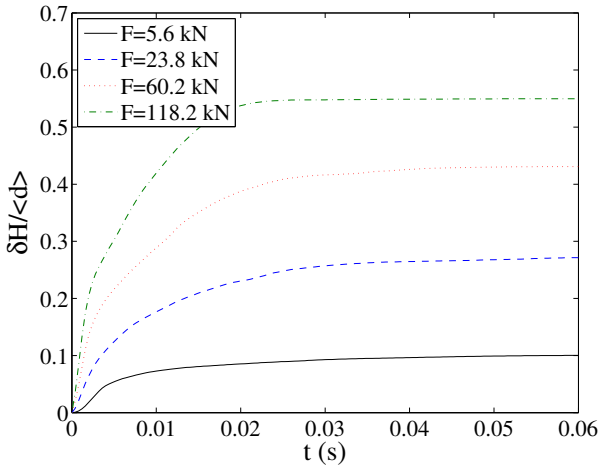

Figure 3: Creep deformation of a sample subjected to different values of the overload F as a function of time.

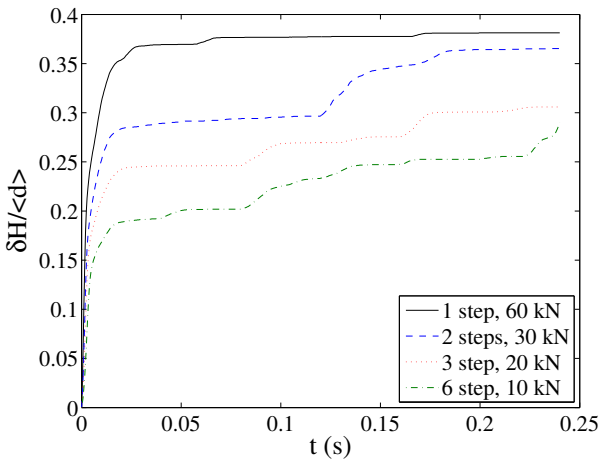

Figure 4: Creep deformation of a sample subjected for a given total overload of 60 kN applied in one and more steps.

The creep deformation depends also on the aspect ratio $\alpha = H_0/D_0$ of the sample. This is mainly due to the fact that the static equilibrium of the sample is controlled both by the internal angle of friction and the friction with the walls at the top and bottom walls (this will be analyzed below).

Fig. 5 shows the time evolution of creep deformation for different samples of different aspect ratios α for the same overload. Larger aspect ratios lead to larger creep deformation.

Finally, the creep deformation shows sample-to-sample fluctuations. Fig. 6 shows the time evolution of creep deformation for the same values of η and aspect ratio α but for different initial configurations. The total deformation ΔH is different. The initially configurations have slightly different values of packing fraction. This difference cannot explain the large creep fluctuations.

All these data indicate clearly that the settlement due to creep deformation depends on various parameters (stress ratio, aspect ratio, loading history) and shows intrinsic fluctuations (depending on subtle details of the microstructure), which can be considered as resulting from a stochastic process.

In the following, we first consider the mean behavior by averaging over different realizations of creep deformations as a function of the stress ratio and and aspect ratio for a given protocol of loading history. Then, we focus on the fluctuations and sample-to-sample variability.

4 Parametric study

In this section, we focus on the joint effects of stress ratio η and aspect ratio α on the total creep deformation.

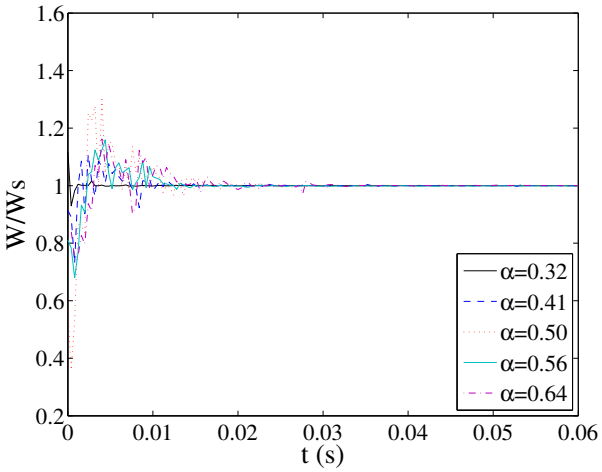

Figure 5: Time evolution of creep deformation for the different samples of different aspect ratios α for the same overload $F = 60kN$.

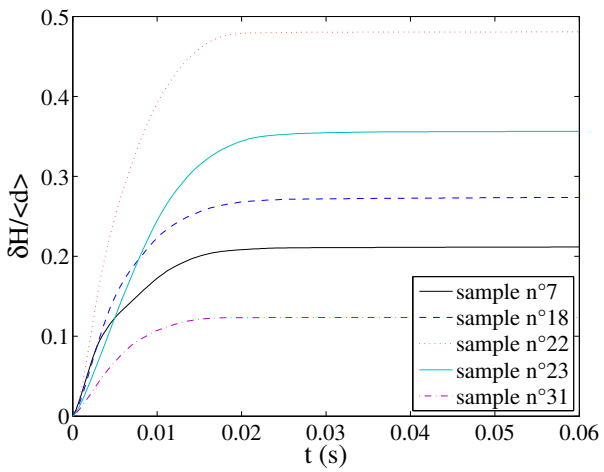

Figure 6: Time evolution of creep deformation for the same values of η and aspect ratio α but for different initial configurations.

Fig. 7 shows the total settlement ΔH as a function of η for the same initial configuration and for $\alpha = 0.5$. We observe that ΔH increases with η in two steps. ΔH only slightly with η until $\eta \simeq 0.5$, then grows much faster for higher η.

The rather low creep deformation below $\eta = 0.5$ is mainly localized at the interface with the top wall where the packing fraction lower and the contact between the wall and the grains is ensured by a rather lower number of contacts. Only for $\eta > 0.5$, the deformation propagates into the bulk of the sample. This point will be analyzed in connection with creep variability below. This creep can be suppressed by pre-loading (pre-consolidation) the sample and allowing the sample to relax. Pre-loading levels out and homogenizes the interface and allows for a more uniform deformation of the sample. Fig. 7 shows the total plastic deformation as a function of η for $\alpha = 0.5$ and after a pre-consolidation of the sample with a load of $F = 3.6$ KN. We see that the initial low creep has disappeared. This effect reflects the plasticity of the material. The pre-consolidation modifies the microstructure not only at the wall interface but also in the bulk. Beyond $\eta = 0.5$, the pre-consolidation has no effect as the microstructure does not evolve anymore with loading.

The joint effect of the stress ratio η and aspect ratio α on the total creep deformation for a sample is displayed in grey level in Fig. 8. The isovalues of creep show clearly that the same level of creep deformation can be reached with a low stress ratio at high aspect ratios or with a high stress ratio at low aspect ratios.

The observed dependence of creep deformation on the aspect ratio is a consequence of friction with the top and bottom walls. The deformation of the packing can be viewed as a radial "extrusion" of the material under vertical forcing. This radial spreading of the material causes a radial mobilization of friction that plays a major role in the equilibrium.

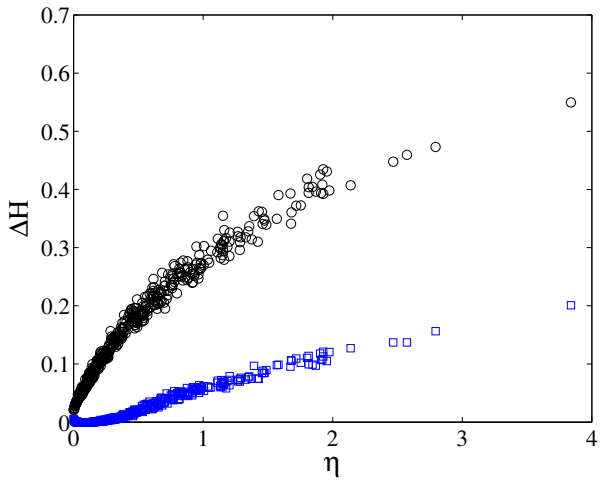

Figure 7: Total creep deformation as a function of η for the initial configuration before and after the pre-loading.

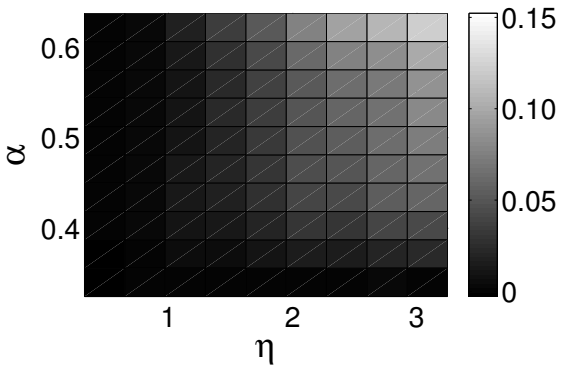

Figure 8: The isovalues of total creep deformation as a function of η and α

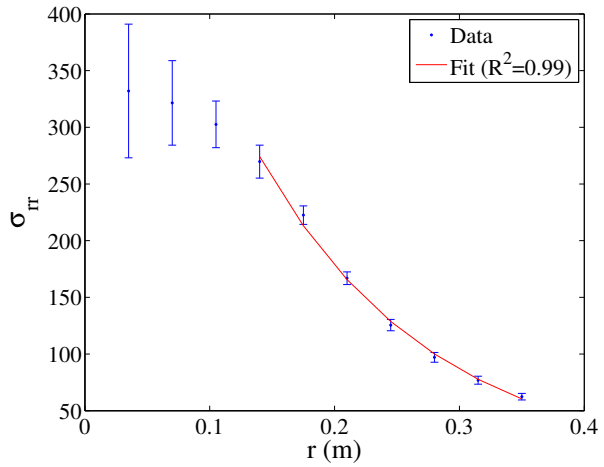

Figure 9: Radial stress as a function of the distance to the symmetry axis of the sample.

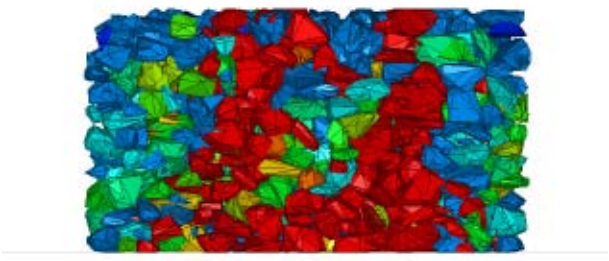

Figure 10: A snapshot of the grain stresses in a vertical section of the sample passing through the axis of symmetry.

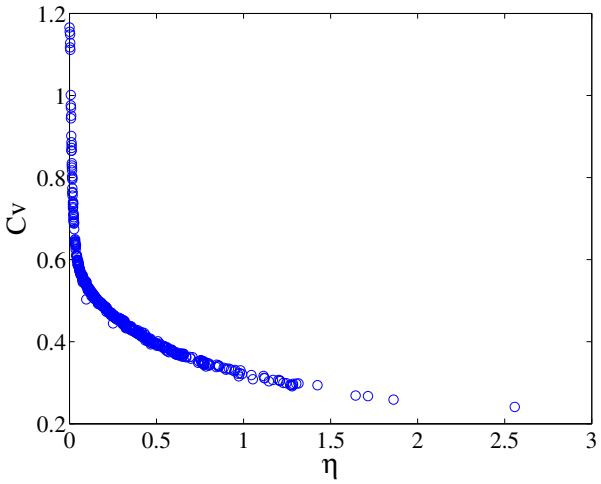

Figure 11: Coefficient of variation of the total creep deformation as a function of stress ratio.

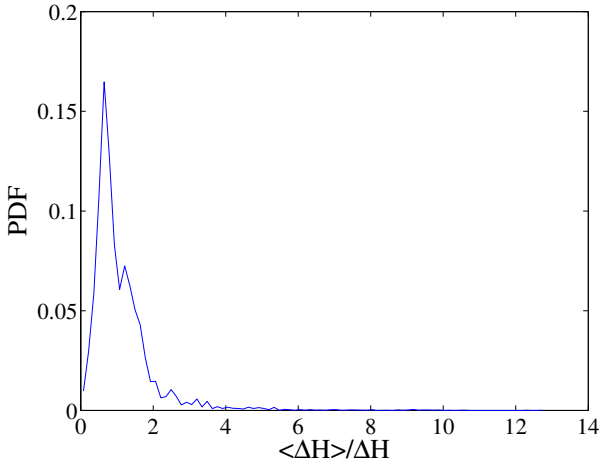

Figure 12: The probability density function of creep deformations in different samples normalized by the mean creep deformation for each value of stress ratio.

We propose here a simple calculation of internal stresses by assuming that the friction is fully mobilized at the walls and inside the material as in the Jansen model for a silo. This model predicts an exponential fall-off of the stress components from the center of the cylindrical sample towards its periphery. Fig. 9 shows the radial stress σ_{rr} estimated from the data as a function of the distance r from the central axis. These data are in good agreement with an exponential fall-off of the stress in exception to the central part where the stresses are over-estimated.

Higher stresses at the center of the sample means that the strongest force chains occur at the center of the sample. This can be seen in a snapshot of the particle stresses displayed in Fig. 10.

5 Creep variability

In order to evaluate the variability of creep deformation, we generated 32 independent configurations of the same aspect ratio α by the same protocol and subjected them to 500 different values of stress ratio η. Fig. 12 shows the coefficient of variation $C_v = \langle \Delta H(\eta) \rangle / S_N(\eta)$ as a function of η. We see in that C_v declines in the range $\eta \in [0, 0.5]$ and then remains almost constant. The high variability in the range $[0, 0.5]$ is related to the low values of the mean creep deformation and reflects the fact that the grain/wall interface varies statistically more in different samples than the bulk structure.

Fig. 13 shows the probability density function of the creep deformation for all samples where the deformations are normalized by the mean deformation for each value of η. The broad distribution of creep deformation declines almost exponentially above the mean. A peak occurs for a values of creep deformation slightly below the mean. This means that the most frequent creep deformation is not the mean creep. Both high creep deformations (the

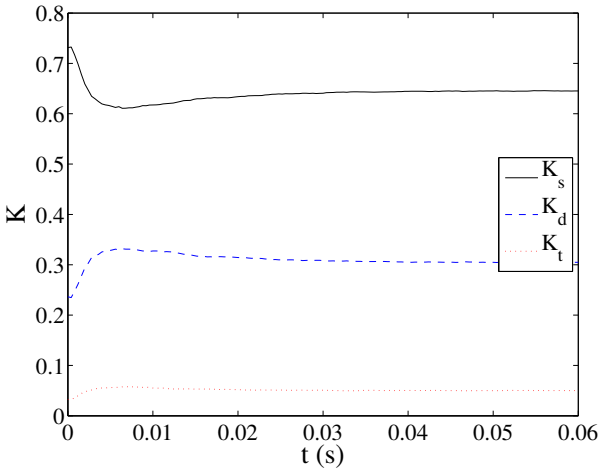

Figure 13: Evolution of the fractions of simple, double and triple contacts with time for $\eta = 2.5$.

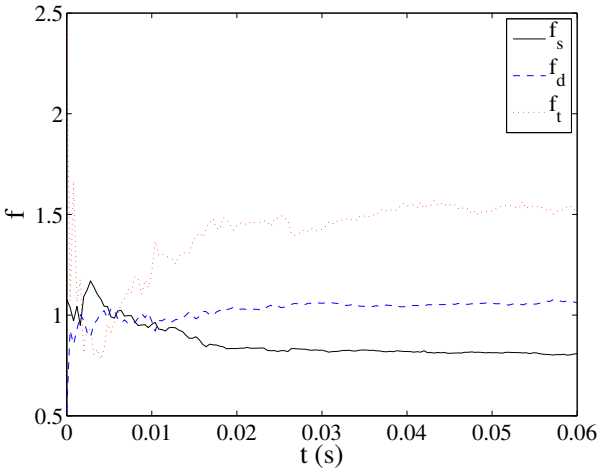

Figure 14: Evolution of the mean force carried by simple, double and triple contacts with time for $\eta = 2.5$.

tail of the distribution) and low creep deformations may occur with significant probability.

6 Fabric variables

The fabric, i.e. the spatial organization of gains and topology of the contact network, encodes most of the past history of loading. In this section, we consider the evolution of several basic fabric variables during creep deformation. These are the mean coordination number Z, the fractions K_s, K_d and K_t of simple, double and triple contacts, respectively, as well as the mean force carried by each type of contact. We show that creep deformation leads to hardening basically as a result of the evolution of the proportions of contact types. In particular, the fraction of triple and double contacts increases, leading to a higher force concentration, whereas Z does not evolve. We also find that K_s is higher than $K_d + K_t$, but f_t and f_t are larger than f_s. This means that the triple contacts concentrate force chains.

REFERENCES

[1] P. A. Cundall and O.D.L. Strack. Discrete numerical model for granular assemblies. *geotechnique*, 29(1):47–65, 1979.

[2] F. Dubois and M. Jean. Lmgc90 une plateforme de développement dédiée à la modélisation des problèmes d'intéraction. In *Actes du sixième colloque national en calcul des structures - CSMA-AFM-LMS* -, volume 1, pages 111–118, 2003.

[3] H. M. Jaeger, S. R. Nagel, and R. P. Behringer. The physics of granular materials. *Physics Today*, 49(4):32–38, 1996.

[4] M. Jean. The non smooth contact dynamics method. In *Special issue on modeling contact and friction*. 1999.

[5] M. Jean and J. J. Moreau. Unilaterality and dry friction in the dynamics of rigid body collections. In *Proceedings of Contact Mechanics International Symposium*, pages 31–48, Lausanne, Switzerland, 1992. Presses Polytechniques et Universitaires Romandes.

[6] J.J. Moreau. *Unilateral contact and dry friction in finite freedom dynamics*, volume 302 of *International Centre for Mechanical Sciences, Courses and Lectures*. Springer, Vienna, 1988.

[7] J.J. Moreau. Some numerical methods in multibody dynamics: Application to granular materials. *European Journal of Mechanics A/Solids*, supp.(4):93–114, 1994. Formulation mathematiques titre du livre Contacts mechanics.

[8] E.G. Nezami, Y.M.A Hashash, D. Zaho, and J. Ghaboussi. A fast contact detection for 3-d discrete element method. *Computers and Geotechnics*, 31:575–587, 2004.

[9] F. Radjaï and E. Azéma. Shear strenght of granular media. *Eur. J. Env. Civil Engineering*, 13:204–218, 2009.

[10] F. Radjai and V. Richefeu. Contact dynamics as a nonsmooth discrete element method. *Mechanics of Materials*, 41:715–728, 2009.

[11] F Radjai, S Roux, and J.J. Moreau. Contact forces in granular packing. *Chaos 9*, pages 544–550, 1999.

[12] G. Saussine. *Contribution à la modélisation de granulats tridimensionnels : application au ballast*. PhD thesis, Université Montpellier II, 2004.

[13] G. Saussine, C. Cholet, P.E. Gautier, F. Dubois, C. Bohatier, and J.J. Moreau. Modelling ballast behaviour under dynamic loading. part 1: A 2d polygonal discrete element method approach. *Computer Methods in Applied Mechanics and Engineering*, 195(19-22):2841–2859, April 2006.